CHEMISTRY
A European Journal

www.chemeurj.org

Reprint

A Journal of
ChemPubSoc Europe
ACES
Asian Chemical Editorial Society
WILEY-VCH

ChemPubSoc Europe

DOI: 10.1002/chem.201805679

CHEMISTRY
A European Journal
Communication

Molecular Evolution |*Hot Paper*|

Increase of Redox Potential during the Evolution of Enzymes Degrading Recalcitrant Lignin

Iván Ayuso-Fernández,[a] Antonio L. De Lacey,[b] Francisco J. Cañada,[a] Francisco J. Ruiz-Dueñas,[a] and Angel T. Martínez*[a]

Abstract: To investigate how ligninolytic peroxidases acquired the uniquely high redox potential they show today, their ancestors were resurrected and characterized. Unfortunately, the transient Compounds I (CI) and II (CII) from peroxide activation of the enzyme resting state (RS) are unstable. Therefore, the reduction potentials ($E^{\circ\prime}$) of the three redox couples (CI/RS, CI/CII and CII/RS) were estimated (for the first time in a ligninolytic peroxidase) from equilibrium concentrations analyzed by stopped-flow UV/Vis spectroscopy. Interestingly, the $E^{\circ\prime}$ of rate-limiting CII reduction to RS increased 70 mV from the common peroxidase ancestor to extant lignin peroxidase (LiP), and the same boost was observed for CI/RS and CI/CII, albeit with higher $E^{\circ\prime}$ values. A straightforward correlation was found between the $E^{\circ\prime}$ value and the progressive displacement of the proximal histidine Hε1 chemical shift in the NMR spectra, due to the higher paramagnetic effect of the heme Fe^{3+}. More interestingly, the $E^{\circ\prime}$ and NMR data also correlated with the evolutionary time, revealing that ancestral peroxidases increased their reduction potential in the evolution to LiP thanks to molecular rearrangements in their heme pocket during the last 400 million years.

The use of paleogenetics to investigate protein properties in evolution is a developing field that has been used to prove different evolutionary hypotheses.[1] Using a robust phylogeny and the ancestral sequence reconstruction tools, the time travel investigation of any family of proteins is virtually possible, even to the early stages of earth.[2] Lignin peroxidases (LiP), versatile peroxidases (VP) and manganese peroxidases (MnP)[3] belong to the peroxidase-catalase superfamily.[4] These fungal heme proteins are characterized by a high reduction potential enabling oxidation of the recalcitrant (non-phenolic) lignin polymer formed by the dehydrogenative polymerization of phenolic monolignols by low redox potential plant peroxidases.[5] Lignin biodegradation, which was defined as an enzymatic combustion,[6] is a key step for carbon recycling in land ecosystems and a process of biotechnological interest for the use of plant biomass in a bio-based economy.[7,8]

The evolutionary changes in ligninolytic peroxidases have been recently investigated[9,10] by resurrection of ancestral enzymes from sequenced genomes of Polyporales,[11] in which most lignin-degrading fungi are included. In this way, the transition from an ancestor that oxidized lignin poorly using diffusible Mn^{3+} chelates, around 400 million years ago,[12] into more efficient enzymes that oxidized lignin directly was demonstrated.[9] That powerful degradative strategy was acquired when a solvent-exposed tryptophanyl radical appeared in an ancestral VP, and became more efficient in ancestral and extant LiPs. The latter include LiP-H8 from the model fungus *Phanerochaete chrysosporium*,[13] corresponding to LiPA (PC-LiPA) in the sequenced genome,[14] the molecular structure of which is shown in Figure 1. Direct degradation of lignin emerged independently several times in peroxidase evolution,[10] showing the importance of lignin decay (by fungi) during land colonization by vascular plants.[12] To elucidate if ligninolytic peroxidases 1) acquired their oxidizing power with evolution or 2) they were already high redox potential enzymes in ancestral Polyporales peroxidases and later shaped their oxidation sites, we analyzed

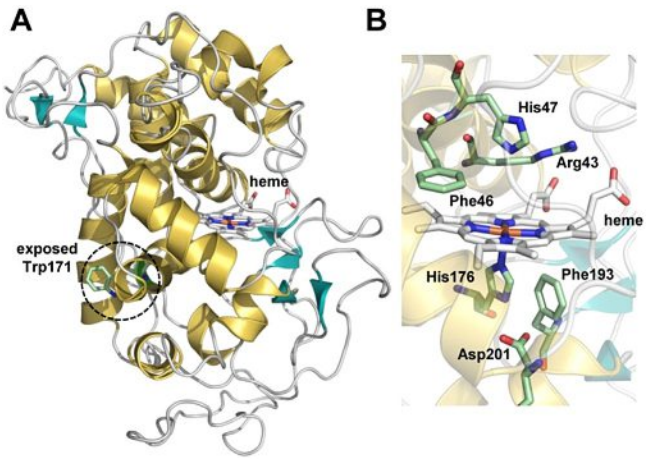

Figure 1. General model of *P. chrysosporium* LiP showing the secondary structure of the protein, the buried heme cofactor and the catalytic tryptophan exposed to the solvent (A), and detail of the heme pocket with two axial histidines and other residues (B). From PDB 1LGA.

[a] *I. Ayuso-Fernández, Prof. Dr. F. J. Cañada, Dr. F. J. Ruiz-Dueñas, Prof. Dr. A. T. Martínez*
Centro de Investigaciones Biológicas, CSIC
Ramiro de Maeztu 9, E-28040, Madrid (Spain)
E-mail: atmartinez@cib.csic.es

[b] *Dr. A. L. De Lacey*
Instituto de Catálisis y Petroleoquímica, CSIC
Marie Curie 2, E-28049 Madrid (Spain)

Supporting information and the ORCID identification number(s) for the author(s) of this article can be found under: https://doi.org/10.1002/chem.201805679.

© 2019 Wiley-VCH Verlag GmbH & Co. KGaA, Weinheim

the evolutionary lineage leading to PC-LiPA (Figure S1, Supporting Information) by ancestral sequence reconstruction from the genomes of ten Polyporales species[11] using the PAML software.[15] The most relevant ancestral sequences in the PC-LiPA lineage were "resurrected", corresponding to: 1) common ancestor of Polyporales peroxidases (CaPo); 2) common ancestor of clade D peroxidases (CaD); 3) first ancestral VP in clade D (AVPd); and 4) first ancestral LiP (ALiP) (multiple alignment in Figure S2, Supporting Information). The four ancestral peroxidases and the extant LiPA were characterized, including the reduction potential estimation for the different redox pairs in the catalytic cycle.

To understand the evolution of the peroxidase redox properties, the three steps of their catalytic cycle[16] were analyzed (Figure 2). The initial reaction is the oxidation of the resting state (RS) enzyme by H_2O_2, extracting two electrons from the cofactor. This generates Compound I (CI) with two oxidizing equivalents (as $Fe^{4+}=O$ and porphyrin cation radical complex).

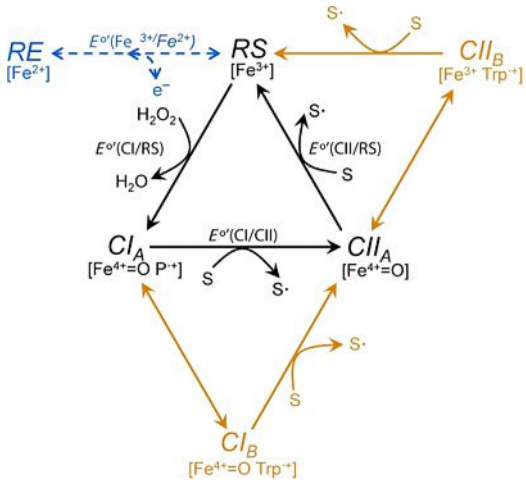

Figure 2. Ligninolytic peroxidase catalytic cycle. Black: the common cycle initiated with oxidation of the RS enzyme by peroxide, followed by two substrate (S) one-electron oxidations (by CI and CII). Orange: the expanded cycle of VPs and LiPs, with formation of a tryptophanyl radical. The blue dashed line leading to the ferrous reduced enzyme (RE-Fe^{2+}) is not part of the cycle, but it has been studied here. The formal reduction potentials ($E^{\circ\prime}$) analyzed are indicated. Adapted from Ref. [17].

Alternatively, CI of LiP/VP transfers one of these equivalents forming the above mentioned solvent-exposed tryptophanyl radical directly oxidizing the bulky lignin polymer,[17,18] which is unable to access the buried cofactor.[19] CI is reduced to Compound II (CII) during oxidation of a substrate molecule. CII has one oxidation equivalent ($Fe^{4+}=O$, in equilibrium with the tryptophanyl radical in LiP/VP), and is further reduced to the RS by oxidation of another molecule of substrate.

The most common redox measurement in heme proteins, basidiomycete peroxidases included,[20–25] is the midpoint potential of the ferric/ferrous transition (Figures S3 and S4, Supporting Information), even though it is not part of the catalytic cycle (Figure 2). To explore the mechanistic implications of reduction potential in the peroxidase catalytic cycle, we used stopped-flow spectrophotometry[26–29] to measure the concentration of the oxidized and reduced forms of the different enzymes in their RS/CI and CII/RS transitions (Figures S5 and S6, respectively) as illustrated in Figure 3 for the most recent ancestor. Stopped flow was used here to assign the equilibrium

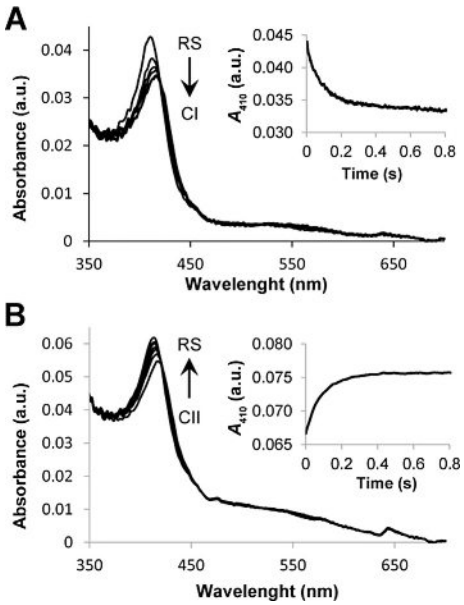

Figure 3. Redox equilibrium analysis by stopped flow. (A) Spectral changes upon rapid mixing of ALiP RS with H_2O_2 to follow CI formation (from 1.6 to 800 ms after peroxide addition). (B) Spectral changes during tyrosine reduction of CII, formed by enzyme mixing with H_2O_2 and ferrocyanide (from 1.6 to 800 ms after tyrosine addition). The insets show time traces at 410 nm (near Soret maximum) to attain equilibrium conditions. All reactions were at the optimal pH 3, and at 25 °C.

concentrations of the two redox states of the enzyme and the two redox states of the substrates used, providing an equilibrium constant that, with the use of the Nerst equation, will allow for the determination of the midpoint potential. In this way, the reduction potentials of the catalytic iron couples (those of CI/RS and CII/RS directly, and the CI/CII $E^{\circ\prime}$ by difference) were calculated for the first time in ligninolytic peroxidases (see Supporting Information, section Supplementary Methods and Tables for details). Analysis of the three half-reactions revealed a general boost of the reduction potentials with evolution (Figure 4). For all the redox pairs (CI/RS, CI/CII and CII/RS) we obtained differences of approximately 70 mV between the oldest ancestor (CaPo) and ALiP, which had the highest reduction potentials (close to the values of extant PC-LiPA).

Starting with the activation by H_2O_2, the $E^{\circ\prime}$(CI/RS) values increase progressively from CaPo (1.34 V) to ALiP (1.41 V), being that value stabilized in extant LiP (Figure 4, center). Although the increasing difficulty to oxidize the enzyme through evolution seems a disadvantage, the reduction potential of this two-electron oxidation is connected to the subsequent one-electron oxidations of substrates[29] [Equation (8) in the Supporting Information, Supplementary Materials and Methods]; the free

© 2019 Wiley-VCH Verlag GmbH & Co. KGaA, Weinheim

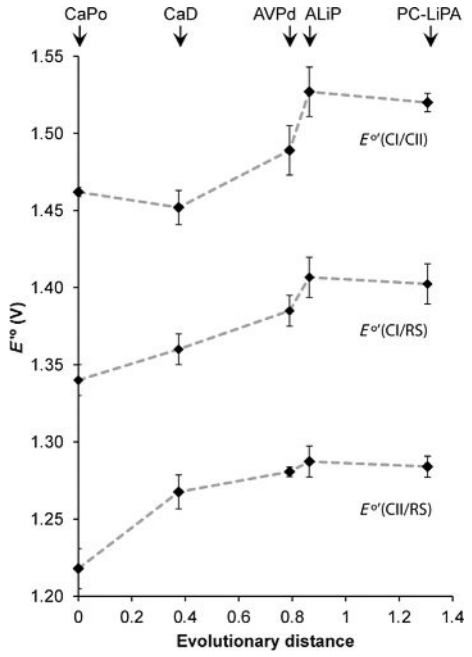

Figure 4. $E^{\circ\prime}$ values for the three redox couples in the catalytic cycle (Figure 2) versus evolutionary distance (see Ref. [10]). The $E^{\circ\prime}$(CI/RS) and $E^{\circ\prime}$(CII/RS) values were from stopped-flow, whereas the $E^{\circ\prime}$(CI/CII) values were from equation $\Delta G_r^{\circ\prime} = -n{\cdot}F{\cdot}E^{\circ\prime}$ (see the Supporting Information).

energy of the activation reaction being the sum of the free energies of the two one-electron oxidations of substrate. Therefore, the higher the $E^{\circ\prime}$(CI/RS), the higher will be the free energy in the subsequent steps, being the oxidation of high redox potential substrates favored in evolution.

The two one-electron oxidations showed strong differences between the $E^{\circ\prime}$(CI/CII) and $E^{\circ\prime}$(CII/RS) values (Figure 4, top and bottom, respectively). Variations of about 0,2 V were observed in all cases, with the $E^{\circ\prime}$(CI/CII) values being the highest, as reported for other peroxidases.[27,29,30] As a result for this high reduction potential, it is expected for CI to be rapidly reduced to CII in the presence of the electron-donor ferrocyanide, as observed in every enzyme analyzed. Moreover, it has been estimated from quantum mechanics/molecular mechanics calculations that, at low pH, the reduction potential would increase due to protonation of negative charges that stabilize CI,[31] with an estimation of $E^{\circ\prime} > 1.2$ V for the PC-LiPA CI/CII couple at pH 3.[32] Here, we estimated for the first time this reduction potential of PC-LiPA at pH 3, the ecophysiological pH of lignin biodegradation in nature,[33] with a value (1.52 V) that widely exceeds those estimations. More importantly, the $E^{\circ\prime}$(CII/RS) also improved in evolution, and the potentials obtained for extant and ancestral peroxidases are the lowest in the catalytic cycle, explaining why this half-reaction is the limiting step in the oxidation of lignin.[17]

The reduction potentials of the three redox couples in extant/ancestral fungal ligninolytic peroxidases are higher than those reported for most animal,[27] plant[34] or prokaryotic[30] peroxidases, usually estimated at pH 7. However, the differences with the $E^{\circ\prime}$ (CI/RS) values of some animal peroxidases,[27] which were estimated with a similar stopped-flow method, would be small after considering the variation (around 0.2 V) existing between the pH 7 and pH 3 estimations,[22,35,36] due to the presence of one or several protonable residues contributing to peroxidase catalysis.[25,37] The values shown here are also slightly higher than the $E^{\circ\prime}$ of 1.3 V estimated at pH 3, with the stopped-flow method, for the CI/RS couple of fungal chloroperoxidase and peroxygenase,[36] two heme-thiolate proteins related to cytochrome P450 monooxygenases.

Additionally, some clues on the structural changes that led to the above boost of reduction potential in the PC-LiPA lineage were provided by ^{1}H NMR spectra of the cyanide adducts of the extant and ancestral enzymes (Figure 5 A), in which the cyanide carbon occupies the position of oxygen in CI/CII, acquired at pH 6.5 to promote enzyme stability and solubility. Analyses under similar conditions have shown that the strength of the bond between the proximal histidine (His176)

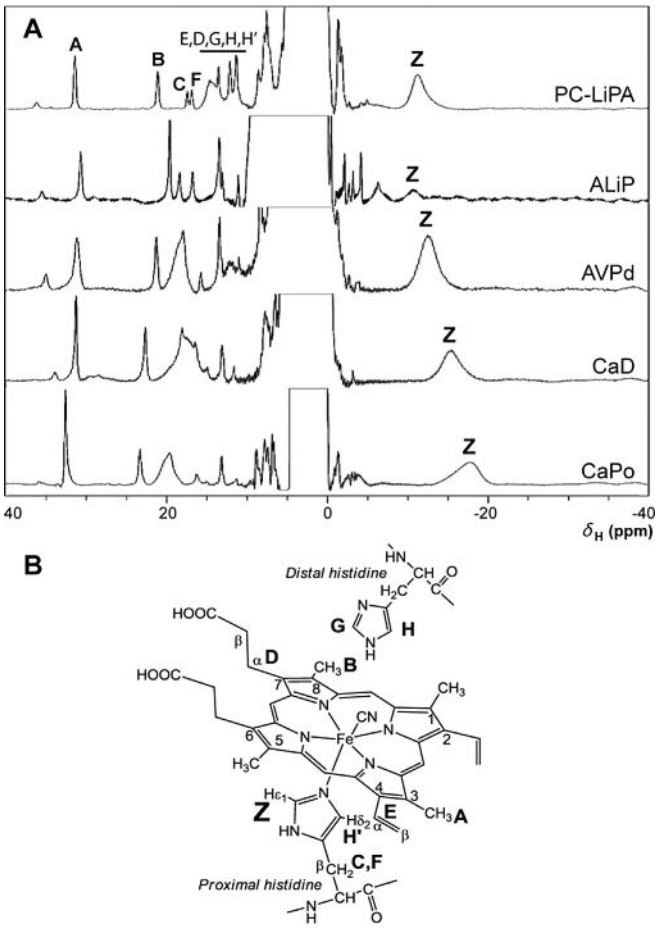

Figure 5. (A) ^{1}H NMR spectra of CN adducts of the ancestral and extant enzymes. Some signals were assigned by comparison with the literature. By homology, in all enzymes the signal Z with the largest high field shift was assigned to the Hε1 of the proximal histidine directly coordinated to the heme Fe^{3+}, whereas the other low-field shifted labeled signals (>10 ppm), correspond to the heme $3CH_3$ (A), $8CH_3$ (B), 7α (D) and 4α (E), the proximal histidine Hβ (C), Hβ′ (F) and Hδ2 (H′) and the distal histidine Hε1(G) and Hδ2(H). Spectra (in 50 mM phosphate, pH 6.5, prepared with ^2H_2O) were acquired with high scanning rate using water eliminated Fourier transform (WEFT) pulse sequence (Ref. [47]) with a short delay to maximize fast relaxing signals. (B) Representation of heme–CN complex as well as proximal and distal histidines, with numbering and labels, as in Ref. [38] by Banci et al..

© 2019 Wiley-VCH Verlag GmbH & Co. KGaA, Weinheim

and the heme Fe^{3+}, and the geometry of the complex (Figure 5B), would influence the redox properties of heme peroxidases, from ancient peroxidases of prokaryotic origin to the more recent peroxidases of basidiomycetes,[38–42] by controlling the imidazolate character of the histidine and the electron deficiency of the iron. The above correlates with the characteristic hyperfine chemical shifts of imidazole protons. These strong hyperfine shifts, induced by the iron paramagnetism, have been extensively used to assign the ^{1}H NMR signals on the amino acids surrounding the heme group in the peroxidases.[43,44] Interestingly, the ring protons of proximal histidine appear as very broad signals, being the Hε1 isolated and located in the upfield area, whereas the Hδ2 is located in the more crowded downfield area.[45,46]

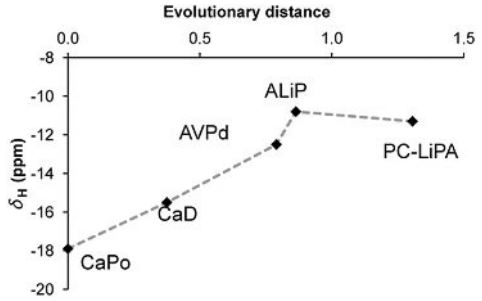

Figure 6. Representation of the evolutionary distance of the ancestral and extant enzymes (Ref. [10]) using the chemical shift (δ_H) of signal Z in the ^{1}H NMR spectra of their CN adducts, which is shown in Figure 5.

Here, we show a significant change in evolution of the Hε1 chemical shift of the proximal histidine (Figure 6), and the same trend was found at pH 3 (not shown) despite the lower peroxidase stability than that at pH 6.5. The gradual δ_H displacement from CaPo (−18 ppm) to ALiP/PC-LiPA (−11 ppm) correlates with a reduction of the imidazolate character of the proximal histidine[40] (due to changes in side-chain distance and/or orientation caused by variable heme/histidine environments) indicative of a weaker axial bond between the histidine side chain and the heme Fe^{3+}, which, in turns, destabilizes the higher oxidation state of the heme iron.[38] Interestingly, this change correlates with the changes observed in the reduction potentials: progressively higher $E^{\circ\prime}$ for the three steps in the peroxidase cycle. This is uniquely interesting, considering that it is the first time that structural data from NMR are correlated with reduction potential measurements of the catalytic cycle couples. Moreover, NMR and stopped-flow changes correlate also with evolutionary time from the common ancestor of Polyporales peroxidases about 400 million years ago.[12] This leads to the main conclusion that, during this period, ligninolytic peroxidases increased their already high redox potential by molecular rearrangement in the proximal side of the heme pocket.

The general boost of reduction potentials sums to other adaptations reported in ligninolytic peroxidase evolution. It has been demonstrated that these enzymes became more stable at acidic pH, at which they act in nature,[33] when they acquired the solvent-exposed tryptophan that oxidize lignin directly.[9] The environment surrounding this tryptophan was also shaped in evolution increasing the oxidation power of the tryptophanyl radical and stabilizing the substrate radical cation intermediates. In particular, the more than five-fold higher efficiency of PC-LiPA oxidizing the simple lignin model compound veratryl alcohol can be connected with the above environment, which is more negative than in its ancestors.[10] Therefore, it seems that, once a high enough reduction potential had been attained (in ALiP), the peroxidase final evolutionary step focused on increasing the acidic stability and selecting a more acidic tryptophanyl radical environment in extant LiP. As a whole, ancestral enzyme resurrection illustrates how LiPs became the most efficient enzymes degrading lignin.

The present study provides new information on the uniquely high reduction potential of enzymes of biotechnological interest due to their ability to degrade lignin, a key issue in lignocellulose biorefineries for the production of bio-based chemicals, fuels and materials.[7]

Experimental Section

Methods: The 113 sequences of class-II peroxidases[4] in the genomes of *Bjerkandera adusta*, *Ceriporiopsis subvermispora*, *Dichomitus squalens*, *Fomitopsis pinicola*, *Ganoderma sp.*, *Phlebia brevispora*, *P. chrysosporium*, *Postia placenta*, *Trametes versicolor* and *Wolfiporia cocos*,[11] available at the DOE JGI (https://genome.jgi.doe.gov/programs/fungi/index.jsf), were used in this study. After sequence alignment with MUSCLE as implemented in Mega X,[48] ML phylogeny was constructed with RAxML,[49] and PAML 4.7[15] was used to obtain the most probable ancestral sequences, which were manually corrected for insertions or deletions, and synthesized for *E. coli* expression. The coding DNA sequences of ancestral and extant peroxidases were cloned and used to transform *E. coli*, and expressed and purified as previously described.[9] $E^{\circ\prime}$ values of the catalytic cycle were calculated using stopped-flow spectrophotometry,[26–29] using tyrosine as reducing substrate, and the $E^{\circ\prime}$ (Fe^{3+}/Fe^{2+}) was obtained through spectrophotometric titration.[22]. ^{1}H NMR spectra of CN adducts of all enzymes were collected, as previously reported for other heme peroxidases,[38] to analyze the displacement with evolution of the signals corresponding to the proximal histidine. For more details see the Supporting Information.

Acknowledgements

This work has been funded by the EnzOx2 (BBI-PPP-2015-2-720297; www.enzox2.eu) EU project, and the CTQ2015-71290-R, BFU2016-77835-R and BIO2017-86559-R projects of the Spanish Ministry of Economy, Industry and Competitiveness, cofinanced by FEDER funds. The NMR service of CIB and M. Carmen Fernández are acknowledged for acquiring the NMR spectra. The authors thank Paul G. Furtmüller and Roland Ludwig (BOKU, Vienna) for advice in stopped-flow determination of reduction potentials, and Werner Mäntele (University of Frankfurt) for kindly providing the spectroelectrochemical cell.

© 2019 Wiley-VCH Verlag GmbH & Co. KGaA, Weinheim

Conflict of interest

The authors declare no conflict of interest.

Keywords: ancestral enzymes · molecular evolution · protein NMR · redox chemistry · stopped–flow equilibrium

[1] Y. Gumulya, E. M. J. Gillam, *Biochem. J.* **2017**, *474*, 1.
[2] V. A. Risso, J. A. Gavira, D. F. Mejia-Carmona, E. A. Gaucher, J. M. Sanchez-Ruiz, *J. Am. Chem. Soc.* **2013**, *135*, 2899 – 2902.
[3] F. J. Ruiz-Dueñas, M. Morales, E. García, Y. Miki, M. J. Martínez, A. T. Martínez, *J. Exp. Bot.* **2009**, *60*, 441 – 452.
[4] M. Zámocký, S. Hofbauer, I. Schaffner, B. Gasselhuber, A. Nicolussi, M. Soudi, K. F. Pirker, P. G. Furtmüller, C. Obinger, *Arch. Biochem. Biophys.* **2015**, *574*, 108 – 119.
[5] G. Battistuzzi, M. Bellei, C. A. Bortolotti, M. Sola, *Arch. Biochem. Biophys.* **2010**, *500*, 21 – 36.
[6] T. K. Kirk, R. L. Farrell, *Annu. Rev. Microbiol.* **1987**, *41*, 465 – 505.
[7] A. T. Martínez, F. J. Ruiz-Dueñas, M. J. Martínez, J. C. del Río, A. Gutiérrez, *Curr. Opin. Biotechnol.* **2009**, *20*, 348 – 357.
[8] A. J. Ragauskas, G. T. Beckham, M. J. Biddy, R. Chandra, F. Chen, M. F. Davis, B. H. Davison, R. A. Dixon, P. Gilna, M. Keller, P. Langan, A. K. Naskar, J. N. Saddler, T. J. Tschaplinski, G. A. Tuskan, C. E. Wyman, *Science* **2014**, *344*, 1246843.
[9] I. Ayuso-Fernández, A. T. Martínez, F. J. Ruiz-Dueñas, *Biotechnol. Biofuels* **2017**, *10*, 67.
[10] I. Ayuso-Fernández, F. J. Ruiz-Dueñas, A. T. Martínez, *Proc. Natl. Acad. Sci. USA* **2018**, *115*, 6428 – 6433.
[11] F. J. Ruiz-Dueñas, T. Lundell, D. Floudas, L. G. Nagy, J. M. Barrasa, D. S. Hibbett, A. T. Martínez, *Mycologia* **2013**, *105*, 1428 – 1444.
[12] D. Floudas, M. Binder, R. Riley, K. Barry, R. A. Blanchette, B. Henrissat, A. T. Martínez, R. Otillar, J. W. Spatafora, J. S. Yadav, A. Aerts, I. Benoit, A. Boyd, A. Carlson, A. Copeland, *Science* **2012**, *336*, 1715 – 1719.
[13] K. E. Hammel, D. Cullen, *Curr. Opin. Plant Biol.* **2008**, *11*, 349 – 355.
[14] D. Martinez, L. F. Larrondo, N. Putnam, M. D. Gelpke, K. Huang, J. Chapman, K. G. Helfenbein, P. Ramaiya, J. C. Detter, F. Larimer, P. M. Coutinho, B. Henrissat, R. Berka, D. Cullen, D. Rokhsar, *Nat. Biotechnol.* **2004**, *22*, 695 – 700.
[15] Z. H. Yang, *Mol. Biol. Evol.* **2007**, *24*, 1586 – 1591.
[16] T. L. Poulos, *Chem. Rev.* **2014**, *114*, 3919 – 3962.
[17] V. Sáez-Jiménez, M. C. Baratto, R. Pogni, J. Rencoret, A. Gutiérrez, J. I. Santos, A. T. Martínez, F. J. Ruiz-Dueñas, *J. Biol. Chem.* **2015**, *290*, 23201 – 23213.
[18] V. Sáez-Jiménez, J. Rencoret, M. A. Rodríguez-Carvajal, A. Gutiérrez, F. J. Ruiz-Dueñas, A. T. Martínez, *Biotechnol. Biofuels* **2016**, *9*, 198.
[19] F. J. Ruiz-Dueñas, A. T. Martínez, *Microb. Biotechnol.* **2009**, *2*, 164 – 177.
[20] G. Battistuzzi, M. Bellei, F. De Rienzo, M. Sola, *J. Biol. Inorg. Chem.* **2006**, *11*, 586 – 592.
[21] C. Ciaccio, A. Rosati, G. De Sanctis, S. Marini, R. Santucci, P. Ascenzi, K. G. Welinder, M. Coletta, *J. Biol. Chem.* **2003**, *278*, 18730 – 18737.
[22] C. D. Millis, D. Cai, M. T. Stankovich, M. Tien, *Biochemistry* **1989**, *28*, 8484 – 8489.
[23] M. Oyadomari, H. Shinohara, T. Johjima, H. Wariishi, H. Tanaka, *J. Mol. Catal. B-Enzym.* **2003**, *21*, 291 – 297.
[24] R. E. Whitwam, R. S. Koduri, M. Natan, M. Tien, *Biochemistry* **1999**, *38*, 9608 – 9616.
[25] R. Santucci, C. Bongiovanni, S. Marini, R. del Conte, M. Tien, L. Banci, M. Coletta, *Biochem. J.* **2000**, *349*, 85 – 90.
[26] M. Sørlie, L. C. Seefeldt, V. D. Parker, *Anal. Biochem.* **2000**, *287*, 118 – 125.
[27] J. Arnhold, P. G. Furtmüller, G. Regelsberger, C. Obinger, *Eur. J. Biochem.* **2001**, *268*, 5142 – 5148.
[28] P. G. Furtmüller, J. Arnhold, W. Jantschko, H. Pichler, C. Obinger, *Biochem. Biophys. Res. Commun.* **2003**, *301*, 551 – 557.
[29] P. G. Furtmüller, J. Arnhold, W. Jantschko, M. Zederbauer, C. Jakopitsch, C. Obinger, *J. Inorg. Biochem.* **2005**, *99*, 1220 – 1229.
[30] I. Efimov, N. D. Papadopoulou, K. J. McLean, S. K. Badyal, I. K. Macdonald, A. W. Munro, P. C. E. Moody, E. L. Raven, *Biochemistry* **2007**, *46*, 8017 – 8023.
[31] L. Castro, L. Crawford, A. Mutengwa, J. P. Goetze, M. Buehl, *Org. Biomol. Chem.* **2016**, *14*, 2385 – 2389.
[32] P. J. Kersten, B. Kalyanaraman, K. E. Hammel, B. Reinhammar, T. K. Kirk, *Biochem. J.* **1990**, *268*, 475 – 480.
[33] A. T. Martínez, *Enzyme Microb. Technol.* **2002**, *30*, 425 – 444.
[34] Z. S. Farhangrazi, M. E. Fossett, L. S. Powers, W. R. Ellis, *Biochemistry* **1995**, *34*, 2866 – 2871.
[35] C. W. Conroy, P. Tyma, P. H. Daum, J. E. Erman, *Biochimica et Biophysica Acta (BBA)—Protein Structure* **1978**, *537*, 62 – 69.
[36] X. S. Wang, S. Peter, R. Ullrich, M. Hofrichter, J. T. Groves, *Angew. Chem. Int. Ed.* **2013**, *52*, 9238 – 9241; *Angew. Chem.* **2013**, *125*, 9408 – 9411.
[37] I. Yamazaki in *Plant Peroxidases: Biochemistry and Physiology, IV International Symposium 1996; Proceedings* (Eds.: C. Obinger, U. Burner, R. Ebermann, C. Penel, H. Greppin), University of Geneva, Geneva, **1996**, pp. 34 – 41.
[38] L. Banci, I. Bertini, R. Pierattelli, M. Tien, A. J. Vila, *J. Am. Chem. Soc.* **1995**, *117*, 8659 – 8667.
[39] L. Banci, I. Bertini, E. A. Pease, M. Tien, P. Turano, *Biochemistry* **1992**, *31*, 10009 – 10017.
[40] L. Banci, I. Bertini, P. Turano, M. Tien, T. K. Kirk, *Proc. Natl. Acad. Sci. USA* **1991**, *88*, 6956 – 6960.
[41] L. Banci, I. Bertini, P. Turano, J. C. Ferrer, A. G. Mauk, *Inorg. Chem.* **1991**, *30*, 4510 – 4516.
[42] L. Banci, S. Camarero, A. T. Martínez, M. J. Martínez, M. Pérez-Boada, R. Pierattelli, F. J. Ruiz-Dueñas, *J. Biol. Inorg. Chem.* **2003**, *8*, 751 – 760.
[43] I. Bertini, P. Turano, A. J. Vila, *Chem. Rev.* **1993**, *93*, 2833 – 2932.
[44] G. N. La Mar, *IUBMB Life* **2007**, *59*, 513 – 527.
[45] G. N. La Mar, J. S. Deropp, V. P. Chacko, J. D. Satterlee, J. E. Erman, *Biochim. Biophys. Acta* **1982**, *708*, 317 – 325.
[46] J. D. Satterlee, J. E. Erman, *Biochemistry* **1991**, *30*, 4398 – 4405.
[47] T. Inubushi, E. D. Becker, *J. Magn. Reson. (1969-1992)* **1983**, *51*, 128 – 133.
[48] S. Kumar, G. Stecher, M. Li, C. Knyaz, K. Tamura, *Mol. Biol. Evol.* **2018**, *35*, 1547 – 1549.
[49] A. Stamatakis, P. Hoover, J. Rougemont, *Syst. Biol.* **2008**, *57*, 758 – 771.

Manuscript received: November 14, 2018
Accepted manuscript online: December 19, 2018
Version of record online: January 25, 2019

© 2019 Wiley-VCH Verlag GmbH & Co. KGaA, Weinheim

CHEMISTRY
A European Journal

Supporting Information

Increase of Redox Potential during the Evolution of Enzymes Degrading Recalcitrant Lignin

Iván Ayuso-Fernández,[a] Antonio L. De Lacey,[b] Francisco J. Cañada,[a] Francisco J. Ruiz-Dueñas,[a] and Angel T. Martínez*[a]

chem_201805679_sm_miscellaneous_information.pdf

Supporting Information includes supplementary Materials and Methods, Tables on stopped-flow calculation of E°'(CI/RS) of CaPo, CaD, AVPd, ALiP and PC-LiPA (**Tables S1-S5**, respectively) and E°'(CII/RS) of CaPo, CaD, AVPd, ALiP and PC-LiPA (**Tables S6-S10**, respectively**)**, inferred E°'(CI/CII) of CaPo, CaD, AVPd, ALiP and PC-LiPA (**Table S11**), Figures on evolution of ligninolytic peroxidases in Polyporales (**Figure S1**), multiple alignment of ancestral peroxidase sequences (**Figure S2**), spectro-electrochemical titration of the Fe^{3+}/Fe^{2+} couple (**Figure S3**), evolutionary distance *vs* E°'(Fe^{3+}/Fe^{2+}) (**Figure S4**), spectral changes during CI formation (**Figure S5**), and CII reduction (**Figure S6**), and Supporting Information References.

SUPPLEMENTARY MATERIALS AND METHODS

Ancestral sequence reconstruction and enzyme production (resurrection). The ancestral sequences were reconstructed as previously described.[1] Briefly, every class-II peroxidase (113 sequences) annotated in the genomes of ten Polyporales (phylum Basidiomycota)[2] were aligned with MUSCLE to obtain a phylogeny using RAxML[3] (with gamma distribution of parameters under the Whelan and Goldman model of evolution and empirical frequencies). Then, PAML 4.7[4] was used to obtain the most probable sequence of the nodes of interest, and the marginal reconstruction sequences were manually corrected for C-terminal and other insertions/deletions according to the ancestor progeny. The genes were synthesized by ATG:biosynthetics (Merzhausen, Germany) using the most frequent codons for high expression in *Escherichia coli*.

The coding DNA sequences of the selected ancestors (CaPo, CaD, AVPd and ALiP in the simplified phylogenetic tree of Figure 1) and the extant PC-LiPA from the *P. chrysosporium* genome (JGI ID# 2989894)[5] were cloned into pET23b(+) (Novagen). The resulting plasmids were transformed into BL21(DE3)pLysS cells, which were grown at 37ºC in Terrific broth till 0.6 OD_{600}, and four additional hours after addition of 1 mM isopropyl β-D-1-thiogalactopyranoside. The apoenzymes accumulated in inclusion bodies and, after solubilization in 8 M urea, an *in vitro* activation protocol was optimized for the ancestral proteins. The activation conditions for the ancestral enzymes include 0.16 M urea, 5 mM $CaCl_2$, 15 µM hemin, 0.4 mM oxidized glutathione, 0.1 mM dithiothreitol and 0.1 mg/mL of protein in 50 mM Tris-HCl (pH 9.5) while those reported by Doyle and Smith[6] were used for PC-LiPA. The active enzymes were

purified in a Resource-Q column (GE-Healthcare) using a 0-400 mM NaCl gradient in 35 mL, 2 mL/min flow, of 10 mM sodium tartrate (pH 5.5) containing 1 mM $CaCl_2$.

Spectro-electrochemical measurement of Fe^{3+}/Fe^{2+} reduction potential. Electronic absorption spectra showing the characteristic Soret band were measured with a Shimadzu UV-2401PC spectrophotometer. Redox titrations were controlled with a BAS-CV27 potentiostat and a FLUKE 77 Series II voltmeter. The potentials were calculated *vs* the standard hydrogen electrode at pH 7 (Tris/HCl 20 mm with 0.2 M of KCl) and 25 ºC for comparison with the literature. For each measurement, 10 µL of enzyme (0.6-1.0 mM concentration) were placed in an *ad hoc* cell,[7] provided by Prof. Mäntele, with a 6 µm gold mesh (Buckbee-Mears) as working electrode, a platinum plate as auxiliary electrode and a silver/silver chloride reference electrode whose potential was checked prior and after each experiment. The potentiometric titrations were carried out in the presence of 50 µM of the following redox mediators: methylene blue, 2-hydroxy-1,4-naphtoquinone, anthraquinone-1,5-disulfonate, anthraquinone-2-sulfonate, neutral red and benzyl viologen. To quantify the oxidized and reduced enzyme, we took the absorbance at the 410 nm (Fe^{3+}) and 438 nm (Fe^{2+}) maxima, and adjusted the values to the Nernst equation:

$$[1]\ A_{410} = A_{\max 410}\frac{e^{\frac{(E-E^{o\prime})nF}{RT}}}{1+e^{\frac{(E-E^{o\prime})nF}{RT}}}$$

$$[2].\ A_{438} = A_{\max 438}\frac{1}{1+e^{\frac{(E-E^{o\prime})nF}{RT}}}$$

Transient state stopped flow experiments. The enzyme in RS, CI or CII states was followed in a stopped-flow rapid spectrophotometry equipment (Bio-Logic) synchronized with a diode array detector (J&M), and the BioKine software. All experiments were made in 100 mM tartrate, pH 3, at 25 ºC. For CI formation, a typical experiment consisted of mixing 4 µM enzyme with different concentrations of H_2O_2 (1-12 molar equivalents till equilibrium) for 3 seconds. To analyze the reduction of CII to RS, a typical experiment started by mixing 8 µM enzyme with enough equivalents (usually 2) of H_2O_2 and 1 equivalent of potassium hexacyanoferrate(II) (ferrocyanide) during 1 second, to ensure total conversion to CII. After that, adding different concentrations of tyrosine, which is oxidized to tyrosinate radical (Tyr·) by the

peroxidases, allowed to quantify the reduction of CII to RS, measuring up to 1 min. All experiments were at least triplicates.

Standard reduction potentials of CI/RS, CI/CII and CII/RS couples. The formal reduction potentials ($E^{o\prime}$) of CI/RS and CII/RS were calculated using the above-described stopped-flow spectrophotometry,[8;9] and the $E^{o\prime}$ of CI/CII was inferred. In the two former cases, the reduction potential was determined using the Nernst equation at equilibrium:

[3] $\Delta E^{o\prime} = (RT / nF)\ lnK'$

that correlates the difference of reduction potentials between enzyme and substrate with the equilibrium constant *K'*. *R* is equal to 8.31 J K^{-1} mol^{-1}, *T* is set to 298 K, *n* represents the number of electrons transferred in a single reaction step of the redox couple, and *F* (the Faraday constant) is 96,485 J V^{-1} mol^{-1}. *K'* represents the equilibrium constant, and is calculated as follows for the couples CI/RS (equation 4) and CII/RS (equation 5):

[4] $K' = ([H_2O_2][RS])/[CI]$
[5] $K' = ([Tyr^{\cdot}][RS])/([Tyr][CII])$

The different redox species at equilibrium were quantified as follows: i) for the pair CI/RS, the amounts of CI and RS were estimated with their extinction coefficients at 410 nm (see below) at the equilibrium (i.e. when the spectral changes ended, during H_2O_2 addition; see Figure 3A) and the reduction potential for the pair H_2O_2/H_2O at pH 3 ($E^{o\prime}$ = 1.56 V);[10] and ii) for the CII/RS pair, the equilibrium concentrations of CII and RS (see Figure 3B) were calculated using their extinction coefficients at 410 nm, after incubation with different amounts of tyrosine, and the calculated $E^{o\prime}$ = 1.18 V for the pair $Tyr^{\cdot}$/Tyr.[11] The selection of Tyr as substrate was made taking into account that: i) all enzymes of the PC-LiPA lineage were able to oxidize it (data not shown); and ii) it has been previously used to calculate the $E^{o\prime}$ of mammalian peroxidases using a similar approach.[9;12-14]

At a specific wavelength, the absorbance is an additive measurement of those of the individual components of a mixture. Therefore, using the 410 nm (Soret band) extinction coefficients for RS, CI and CII (given below) the quantification of the

different redox pairs at equilibrium is possible using the equations 6 (for equilibrium of CI and RS) and 7 (for equilibrium of CII and RS):

[6] $A_{410} = \varepsilon_{410\text{-}RS}\,[RS]\,l + \varepsilon_{410\text{-}CI}\,[CI]\,l$

[7] $A_{410} = \varepsilon_{410\text{-}CI}\,[CI]\,l + \varepsilon_{410\text{-}CII}\,[CII]\,l$

where l is the path length of the stopped-flow cuvette.

The RS ε_{410} values were: 138 mM^{-1} cm^{-1} (RS-CaPo), 177 mM^{-1} cm^{-1} (RS-CaD), 149 mM^{-1} cm^{-1} (RS-AVPd), 171 mM^{-1} cm^{-1} (RS-ALiP) and 168 mM^{-1} cm^{-1} (RS-PC- LiPA). The CI ε_{410} was calculated after converting all the RS enzyme into CI using 2-10 H_2O_2 equivalents, ensuring there is no auto-reduction to CII. The values obtained were: 53 mM^{-1} cm^{-1} (CI-CaPo), 74 mM^{-1} cm^{-1} (CI-CaD), 68 mM^{-1} cm^{-1} (CI-AVPd), 87 mM^{-1} cm^{-1} (CI-ALiP) and 110 mM^{-1} cm^{-1} (CI- PC-LiPA). The CII ε_{410} was calculated after converting all RS enzyme into CI and then into CII, without further auto-reduction to RS, using 2 equivalents of H_2O_2 and 1 equivalent of ferrocyanide.[15] The values obtained were: 73 mM^{-1} cm^{-1} (CII-CaPo), 98 mM^{-1} cm^{-1} (CII-CaD), 105 mM^{-1} cm^{-1} (CII-AVPd), 133 mM^{-1} cm^{-1} (CII-ALiP) and 105 mM^{-1} cm^{-1} (CII- PC-LiPA).

Concerning the $E^{o'}$ of CI/CII, we were unable to calculate it experimentally. Despite obtaining enzyme in CI and being able to attain certain equilibrium with CII at specific Tyr concentrations, the CII auto-reduction to RS enzyme made impossible to calculate equilibrium concentrations. However, it was possible to infer the $E^{o'}$ of CI/CII from the experimental values of the CI/RS and CII/RS couples. The standard reaction free energy is connected to $E^{o'}$ according to:

[8] $\Delta G_r'^{o} = -n\,F\,E^{o'}$

with n = 2 electrons for the reduction of CI to RS, $\Delta G_r'^{o}$ equals to -2 x F x [$E^{o'}$(CI/RS)] being the sum of the reaction free energy of one electron reductions (CI to CII, and CII to RS). Therefore, the sum of reaction free energies $\Delta G_r'^{o}$(CI/CII) + $\Delta G_r'^{o}$(CII/RS) and the experimental determination of $E^{o'}$(CII/RS) allows the determination of $E^{o'}$(CI/CII).

^{1}H NMR Spectroscopy. The cyanide adducts of the ancestral peroxidases and extant PC-LiPA were obtained by incubating 0.7-1.0 mM of each sample with KCN in 50 mM potassium phosphate, pH 6.5, prepared with ^2H_2O (isotopic purity 99.9%). The ^{1}H-

NMR spectra were recorded at 298K using a 600 MHz Bruker spectrometer equipped with cryoprobe. Fast scanning WEFT pulse sequence was used.[16] Delays between 13 to 120 ms were tested in order to maximize signals corresponding to fast relaxing protons of the proximal histidine coordinated to Fe of the heme group. Spectra were acquired with up to 40K total scans, 120 ppm spectral width and a minimum of 1K points. The spectra were processed with TOPSPIN 3.0 (Bruker) with manual base line adjustment and the signal of residual water proton (δ_H 4.701 ppm) was used as internal reference for chemical shifts.

Precise conditions of the presented spectra are: i) CaPo, addition of 5 spectra of 1K scans and 128 dummy scans each, 15 ms delay, 100 ppm width and 1K points; ii) CaD, addition of 5 spectra of 4K scans and 128 dummy scans each, 13 ms delay, 120 ppm width and 1K points; iii) AVPd, addition of 5 spectra of 1K scans and 128 dummy scans each, 13 ms delay, 120 ppm width and 1K points; iv) AliP, addition of 5 spectra of 4K scans and 128 dummy scans each, 23 ms delay, 100 ppm width and 2K points; and v) PC-LiPA, addition of 10 spectra of 4K scans and 128 dummy scans each, 13 ms delay, 120 ppm width and 1K points.

Signal corresponding to Hε1 of the proximal histidine was assigned to the signal with highest upper-field shift by homology with reported data.[17-21] Other signals were assigned by comparison with reported data for PC-LiPA isolated from *P. chrysosporium* cultures, although some differences are observed as the PC-LiPA used in this study was obtained by heterologous expression in *E. coli* and devoid of natural glycosylation. Heme group numbering and protons labeling are indicated in Figure 5B and correspond to those used by Banci et al.[17]

SUPPLEMENTARY TABLES

Table S1. Parameters of the redox equilibrium and calculated $E^{o'}$ of the CI/RS redox couple of CaPo as a function of the initial concentration of H_2O_2 (all reactions at optimal pH 3).

Initial H_2O_2	Equilibrium concentrations (µM)			$E^{o'}$ (V)
(µM)	CI-CaPo	RS-CaPo	H_2O_2	
2.00	1.73	0.16	0.27	1.334
3.00	1.85	0.05	1.15	1.335
4.00	1.85	0.05	2.16	1.345
8.00	1.87	0.02	6.13	1.339
Mean and 95% confidence interval:				1.338 ± 0.004

Table S2. Parameters of the redox equilibrium and calculated $E^{o'}$ of the CI/RS redox couple of CaD as a function of the initial concentration of H_2O_2 (all reactions at optimal pH 3).

Initial H_2O_2	Equilibrium concentrations (µM)			$E^{o'}$ (V)
(µM)	CI-CaD	RS-CaD	H_2O_2	
1.00	0.77	1.15	0.23	1.369
2.00	1.09	0.83	0.91	1.378
3.00	1.55	0.3	1.45	1.367
4.00	1.83	0.09	2.17	1.353
Mean and 95% confidence interval:				1.367 ± 0.011

Table S3. Parameters of the redox equilibrium and calculated $E^{o'}$ of the CI/RS redox couple of AVPd as a function of the initial concentration of H_2O_2 (all reactions at optimal pH 3).

Initial H_2O_2	Equilibrium concentrations (µM)			$E^{o'}$ (V)
(µM)	CI-AVPd	RS-AVPd	H_2O_2	
1.00	0.28	1.08	0.72	1.392
2.00	0.55	0.81	1.45	1.392
3.00	0.94	0.42	2.06	1.382
4.00	1.18	0.18	2.82	1.372
Mean and 95% confidence interval:				1.385 ± 0.011

Table S4. Parameters of the redox equilibrium and calculated $E^{o'}$ of the CI/RS redox couple of ALiP as a function of the initial concentration of H_2O_2 (all reactions at optimal pH 3).

Initial H_2O_2	Equilibrium concentrations (µM)			$E^{o'}$ (V)
(µM)	CI-ALiP	RS-ALiP	H_2O_2	
1.00	0.06	1.75	0.094	1.429
2.00	0.50	1.31	1.50	1.400
3.00	0.67	1.14	2.33	1.400
4.00	0.77	1.04	3.23	1.402
8.00	1.10	0.71	6.90	1.402
Mean and 95% confidence interval:				1.407 ± 0.011

Table S5. Parameters of the redox equilibrium and calculated $E^{o'}$ of the CI/RS redox couple of PC-LiPA as a function of the initial concentration of H_2O_2 (all reactions at optimal pH 3).

Initial H_2O_2	Equilibrium concentrations (μM)			$E^{o'}$ (V)
(μM)	CI-PCLiPA	RS-PCLiPA	H_2O_2	
1.50	0.27	1.97	1.23	1.411
2.00	0.41	1.85	1.59	1.408
3.00	0.98	1.28	2.02	1.395
4.00	1.14	1.13	2.86	1.396
8.00	1.53	0.73	6.47	1.399
Mean and 95% confidence interval:				1.402 ± 0.006

Table S6. Parameters of the redox equilibrium and calculated $E^{o'}$ of the CII/RS redox couple of CaPo as a function of the initial concentration of Tyr (all reactions at optimal pH 3).

Initial Tyr	Equilibrium concentrations (μM)				$E^{o'}$ (V)
(μM)	RS-CaPo	CII-CaPo	Tyr	Tyr·	
5	0.79	1.35	4.21	0.79	1.233
10	1.22	0.92	8.78	1.22	1.219
25	1.66	0.49	23.35	1.66	1.212
50	1.88	0.26	48.12	1.88	1.207
Mean and 95% confidence interval:					1.217 ± 0.011

Table S7. Parameters of the redox equilibrium and calculated E$^{o\prime}$ of the CII/RS redox couple of CaD as a function of the initial concentration of Tyr (all reactions at optimal pH 3).

Initial Tyr	Equilibrium concentrations (μM)				E$^{o\prime}$ (V)
(μM)	RS-CaD	CII-CaD	Tyr	Tyr·	
2.5	0.35	1.47	2.15	0.35	1.258
5	0.48	1.34	4.52	0.48	1.260
10	0.60	1.22	9.4	0.6	1.264
20	0.60	1.22	19.4	0.6	1.283
Mean and 95% confidence interval:					1.266 ± 0.011

Table S8. Parameters of the redox equilibrium and calculated E$^{o\prime}$ of the CII/RS redox couple of AVPd as a function of the initial concentration of Tyr (all reactions at optimal pH 3).

Initial Tyr	Equilibrium concentrations (μM)				E$^{o\prime}$ (V)
(μM)	RS-AVPd	CII-AVPd	Tyr	Tyr·	
10	0.50	1.85	9.51	0.50	1.286
20	0.79	1.56	19.21	0.79	1.275
50	1.17	1.18	48.83	1.17	1.270
100	1.35	1.00	98.65	1.35	1.278
Mean and 95% confidence interval:					1.278 ± 0.006

Table S9. Parameters of the redox equilibrium and calculated E$^{o'}$ of the CII/RS redox couple of ALiP as a function of the initial concentration of Tyr (all reactions at optimal pH 3).

Initial Tyr	Equilibrium concentrations (μM)				E$^{o'}$ (V)
(μM)	RS-ALiP	CII-ALiP	Tyr	Tyr·	
10	0.46	2.02	9.54	0.46	1.294
20	0.64	1.84	19.36	0.64	1.290
50	1.04	1.44	48.96	1.04	1.283
100	1.35	1.13	98.65	1.35	1.281
Mean and 95% confidence interval:					1.287 ± 0.006

Table S10. Parameters of the redox equilibrium and calculated E$^{o'}$ of the CII/RS redox couple of PC-LiPA as a function of the initial concentration of Tyr (all reactions at optimal pH 3).

Initial Tyr	Equilibrium concentrations (μM)				E$^{o'}$ (V)
(μM)	RS-PCLiPA	CII-PCLiPA	Tyr	Tyr·	
10	0.42	1.50	9.58	0.42	1.289
20	0.62	1.30	19.38	0.62	1.283
50	0.95	0.97	49.05	0.95	1.279
100	1.19	0.73	98.81	1.19	1.277
Mean and 95% confidence interval:					1.284 ± 0.006

Table S11. Eº'(CI/CII) inferred for each enzyme using the equation for the reaction free energy ($\Delta G_r^{o\prime} = -n\ F\ E^{o\prime}$). Eº'(CI/RS) and Eº'(CII/RS) were obtained experimentally at optimal pH 3 (**Tables S1-S5** and **S6-S10**, respectively). For RS/CI n = 2, and its $\Delta G_r^{o\prime}$ equals to the sum of the $\Delta G_r^{o\prime}$(CI/CII) and $\Delta G_r^{o\prime}$(CII/R), both with n = 1.

	$\Delta G_r^{o\prime}$(R/CI) (kJ)	$\Delta G_r^{o\prime}$(CII/R) (kJ)	$\Delta G_r^{o\prime}$(CI/CII) (kJ)	$E^{o\prime}$(CI/CII) (V)
CaPo	-258.6	-117.5	-141.1	1,462
CaD	-262.4	-122.4	-140.1	1,452
AVPd	-267.3	-123.6	-143.7	1,489
ALiP	-271.5	-124.2	-147.3	1,527
PCLiPA	-270.5	-123.9	-146.7	1,520

SUPPLEMENTARY FIGURES

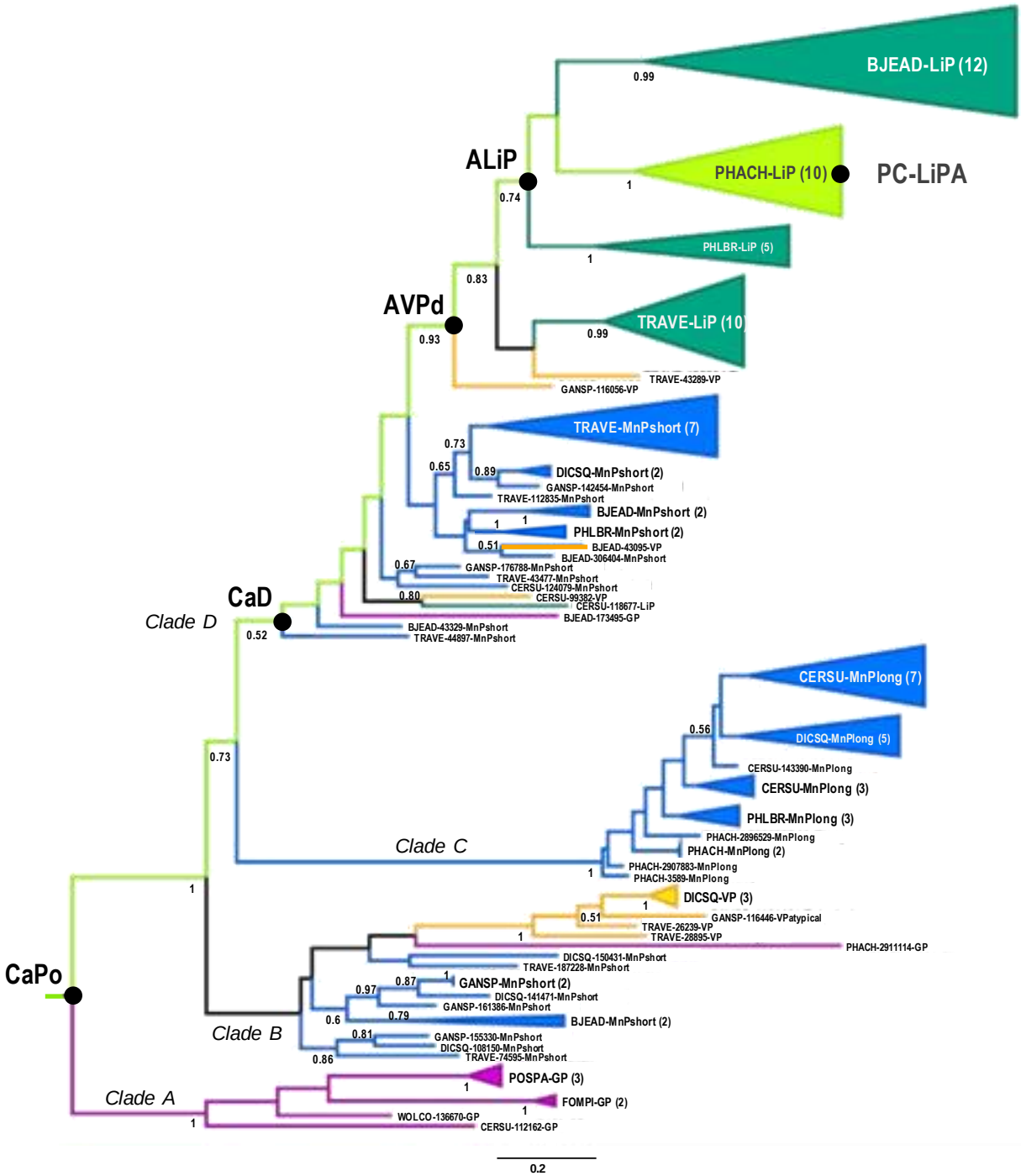

Figure S1. Evolution of fungal ligninolytic peroxidases in Polyporales (bootstrap values > 0.5 are indicated) adapted from Ayuso-Fernández *et al.*[22] LiPs are shown in green, VPs in yellow, MnPs in blue and GPs in purple. The path to the extant LiPA of *P. chrysosporium* (JGI ID# 2989894) is marked in light green. Also, the enzymes analyzed in the present work (common ancestor of Polyporales peroxidases, CaPo; common ancestor of clade D, CaD; ancestral versatile peroxidase in clade D, AVPd; and ancestral LiP, ALiP) are marked.

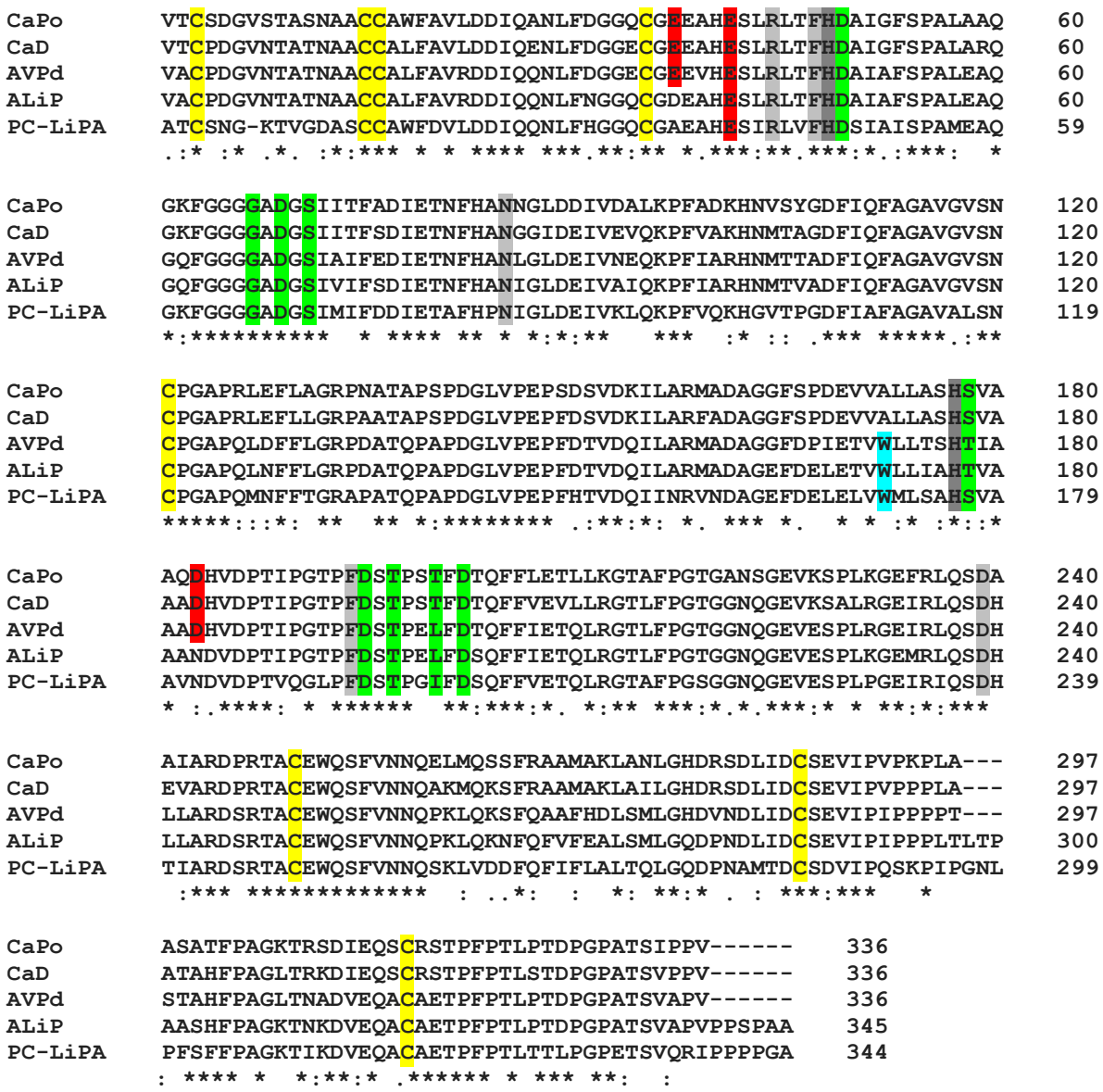

Figure S2. Alignment of the four ancestral sequences (mature proteins) predicted with PAML 4.7 and extant LiPA. Conserved catalytic and other relevant residues[23] are indicated including: two active site histidines (*dark gray*); three acidic residues forming the Mn^{2+}-binding site (*red*); other active site conserved residues (*light gray*); one tryptophan involved in lignin direct oxidation (*cyan*); nine ligands of two Ca^{2+} ions (*green*); and eight cysteines forming disulfide bonds (*yellow*). Symbols below indicate full conservation of the same (*asterisk*) or equivalent residues (*colon*) and partial residue conservation (*dot*). Adapted from Ayuso-Fernández et al.[1]

Figure S3 (next page)**.** Spectro-electrochemical titration of the Fe^{3+}/Fe^{2+} couple in ancestral CaPo (**A**), CaD (**B**), AVPd (**C**) and ALiP (**D**) peroxidases. As described in supplementary Materials and Methods, the use of different redox mediators allowed the conversion of RS-Fe^{3+} to RE-Fe^{2+} after applying several potential differences. All the potentials are referred to the standard hydrogen electrode. The data obtained were fitted to the Nernst equation for a reversible one electron transition. Continuous line: changes in the $A_{410\text{-nm}}$ (Fe^{3+}); dashed line: changes in $A_{438\text{-nm}}$ (Fe^{2+}).

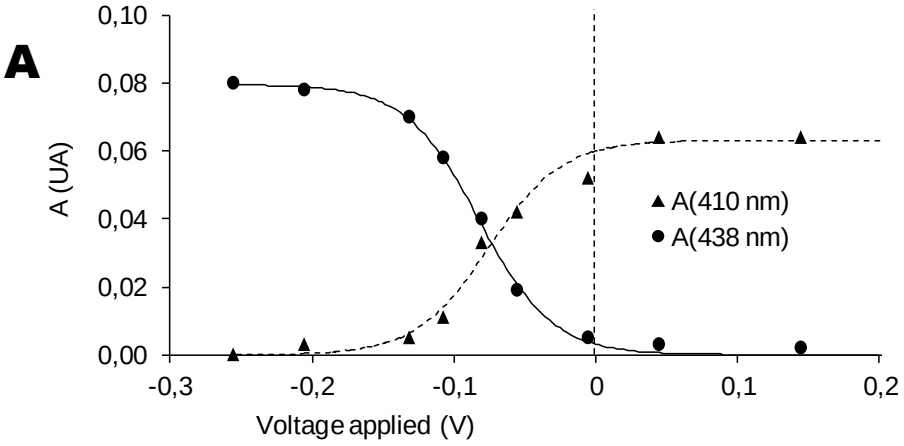
A
0,10
0,08
0,06
0,04
0,02
0,00
A (UA)
A(410 nm)
A(438 nm)
-0,3
-0,2
-0,1
0
0,1
0,2
Voltage applied (V)

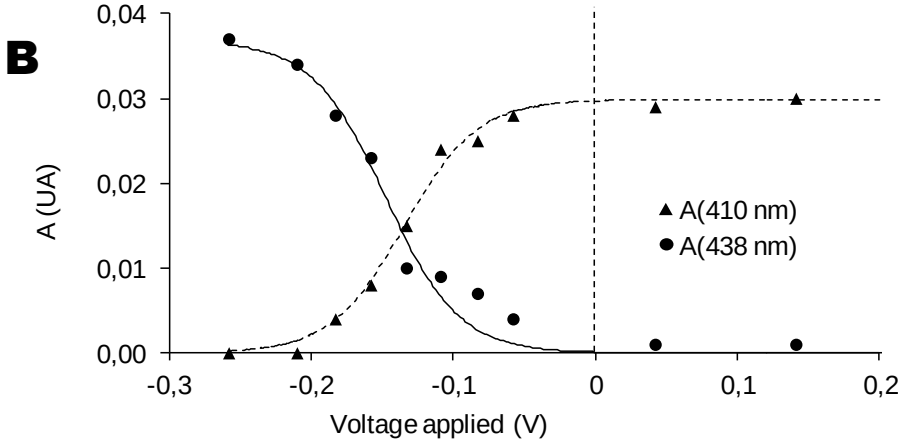
B
0,04
0,03
0,02
0,01
0,00
A (UA)
A(410 nm)
A(438 nm)
-0,3
-0,2
-0,1
0
0,1
0,2
Voltage applied (V)

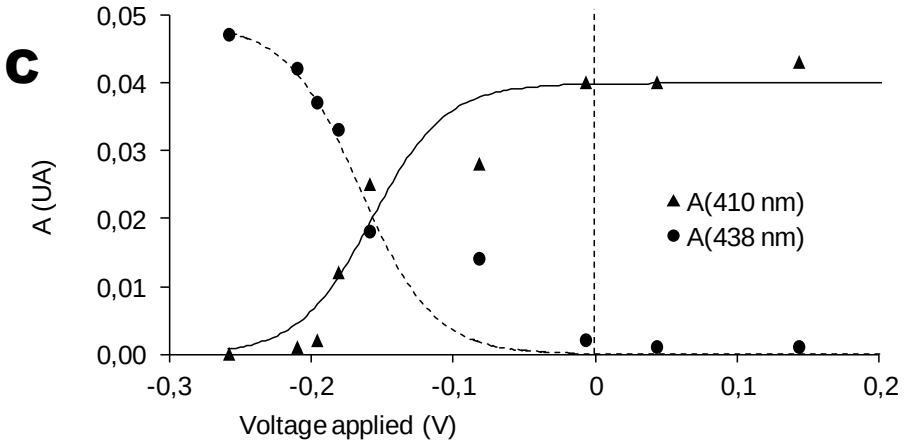
C
0,05
0,04
0,03
0,02
0,01
0,00
A (UA)
A(410 nm)
A(438 nm)
-0,3
-0,2
-0,1
0
0,1
0,2
Voltage applied (V)

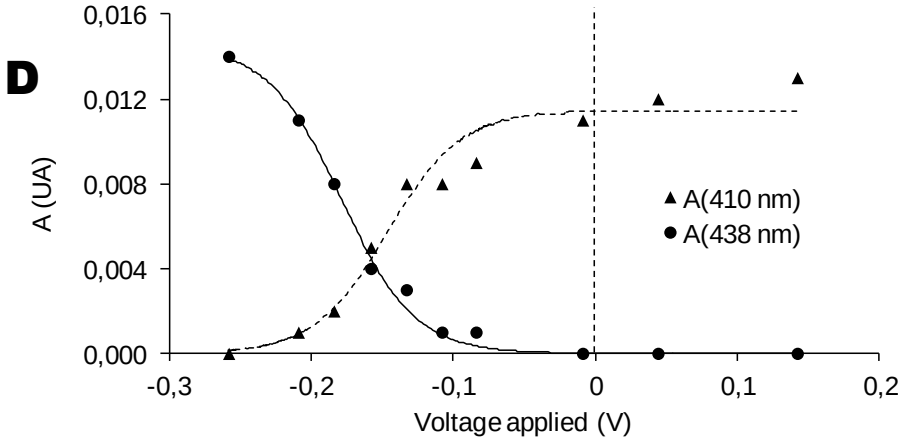
D
0,016
0,012
0,008
0,004
0,000
A (UA)
A(410 nm)
A(438 nm)
-0,3
-0,2
-0,1
0
0,1
0,2
Voltage applied (V)

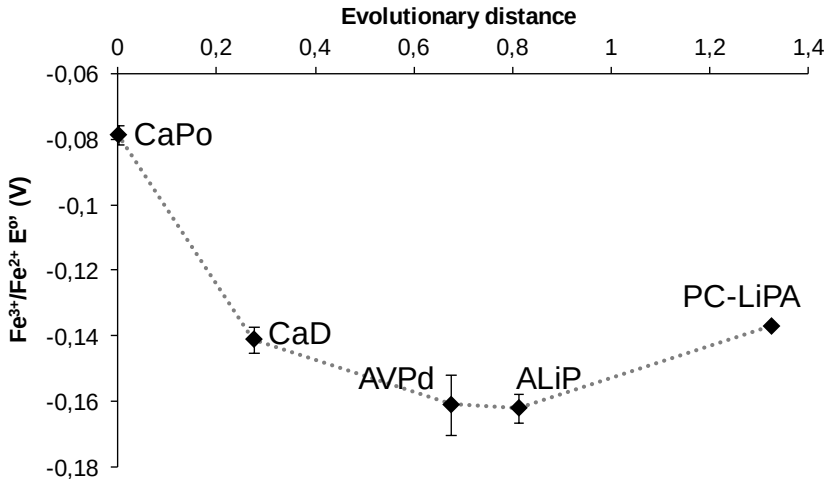

Figure S4. $E^{o'}(Fe^{3+}/Fe^{2+})$ values *vs* evolutionary distance of ancestral peroxidases (CaPo, CaD, AVPd and ALiP) and PC-LiPA. See **Figure S3** for the spectro-electrochemical titration of the ancestral enzymes. The values for PC-LiP have been reported several times in the bibliography, and here we take the most accepted value of -0.137 V.[24] The negative values ensure that the peroxidases have a heme with Fe^{3+}, the active form of iron, being in the range of those reported for other basidiomycete peroxidases.[24-29] Although it is considered that a more positive $E^{o'}$ would mean a higher oxidation power,[12] PC-LiPA, along with AVPd and ALiP, are able to oxidize high redox-potential substrates in spite of the more negative $E^{o'}(Fe^{3+}/Fe^{2+})$ than the evolutionarily older CaPo and CaD, which only oxidize low redox-potential substrates and Mn^{2+},[1] estimated here.

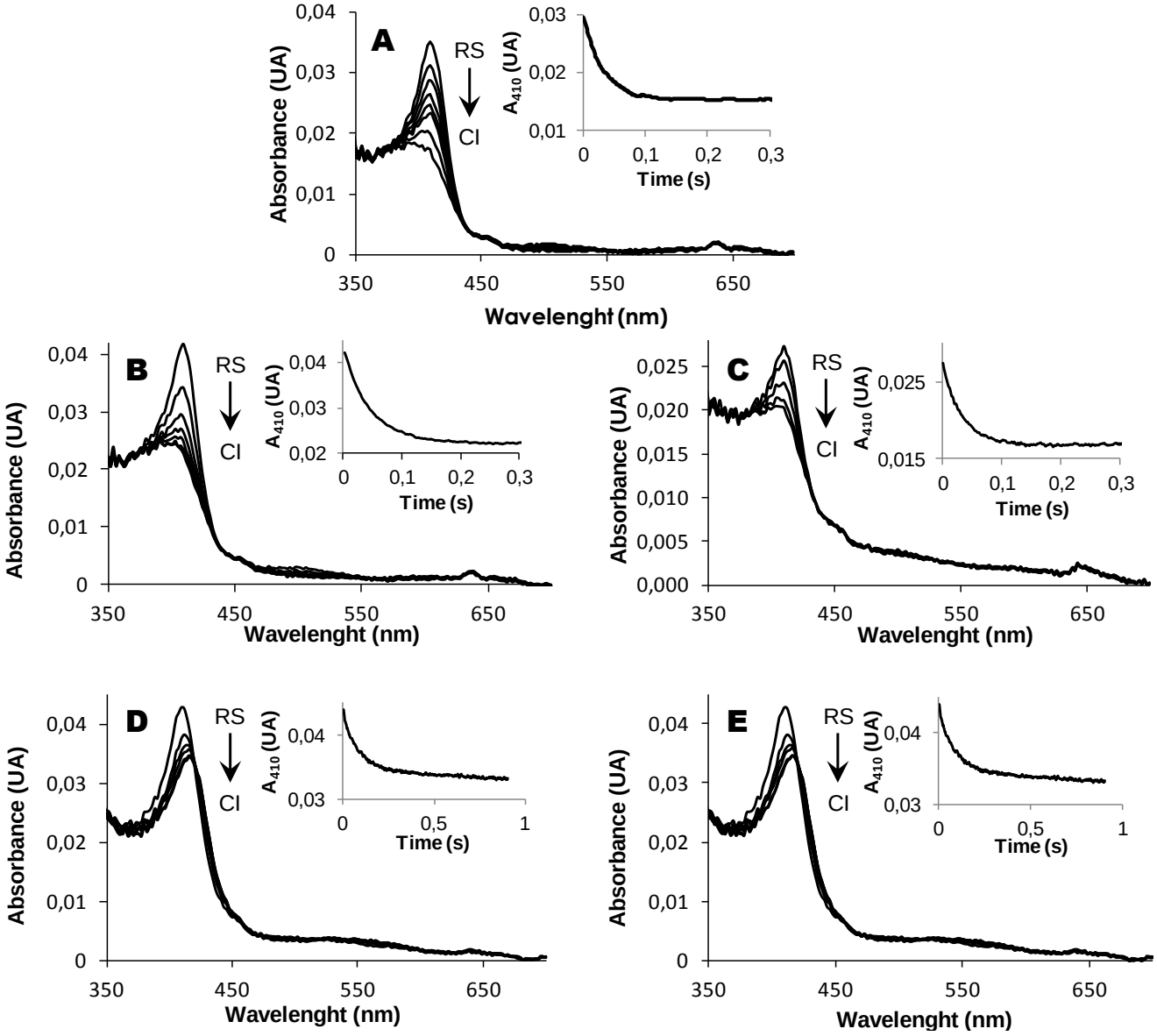

Figure S5. Spectral changes upon mixing of CaPo (**A**), CaD (**B**), AVPd (**C**), ALiP (**D**) and PC-LiPA (**E**) with H_2O_2 to follow CI formation (from 1.6 to 225 ms after peroxide addition). The insets show time traces at 410 nm (near Soret maximum) to attain equilibrium conditions. All reactions were at optimal pH 3, and 25 ºC.

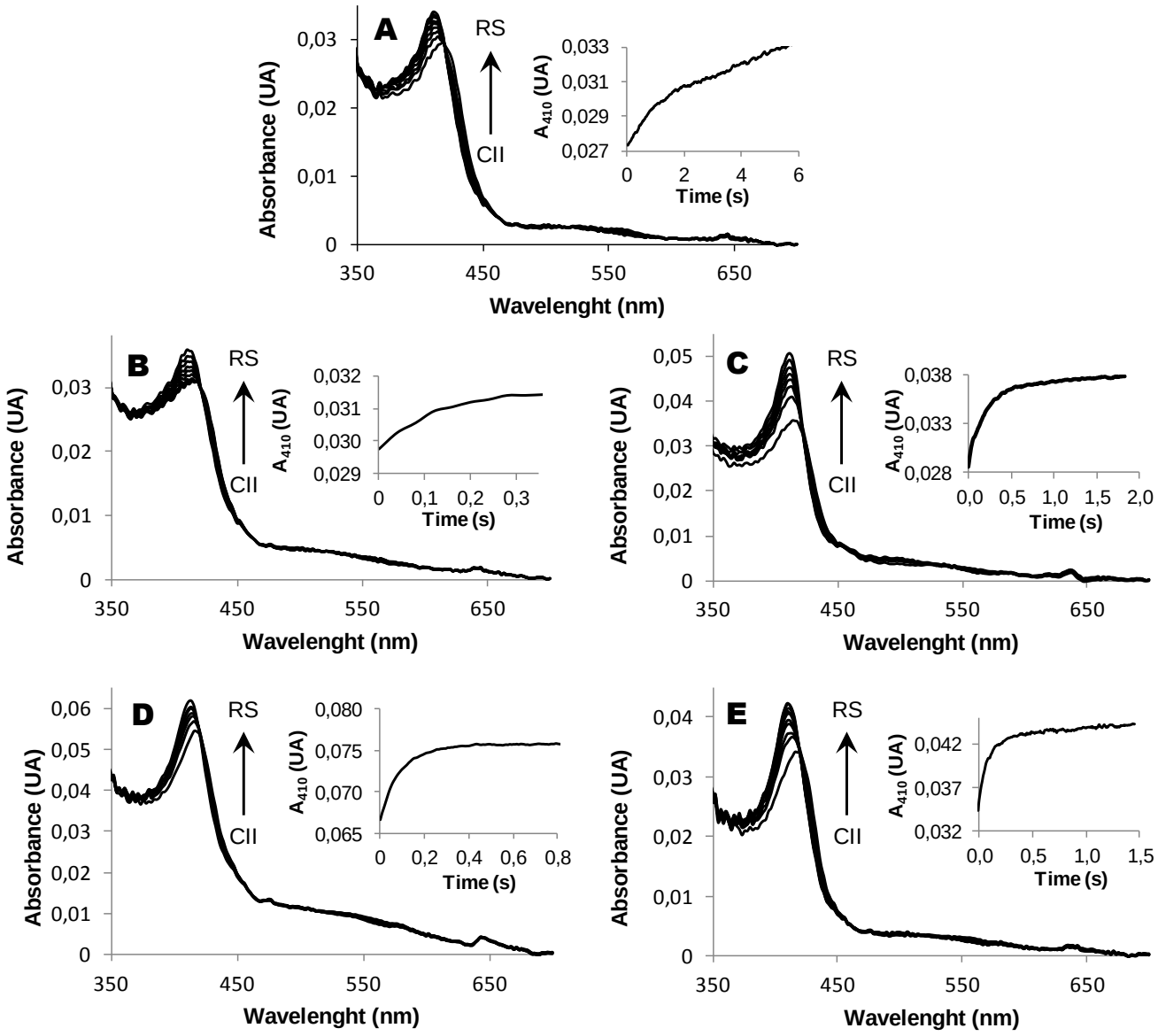

Figure S6. Spectral changes during Tyr reduction of CII, formed by CaPo (**A**), CaD (**B**), AVPd (**C**), ALiP (**D**) and PC-LiPA (**E**) mixing with H_2O_2 and ferrocyanide (from 1.6 to 650 ms after Tyr addition).The insets show time traces at 410 nm (near Soret maximum) to attain equilibrium conditions. All reactions were at optimal pH 3, and 25 ºC.

SUPPORTING INFORMATION REFERENCES

[1] I. Ayuso-Fernández, A. T. Martínez, F. J. Ruiz-Dueñas, *Biotechnol. Biofuels* **2017,** *10,* 67.
[2] F. J. Ruiz-Dueñas, T. Lundell, D. Floudas, L. G. Nagy, J. M. Barrasa, D. S. Hibbett, A. T. Martínez, *Mycologia* **2013,** *105,* 1428-1444.
[3] A. Stamatakis, P. Hoover, J. Rougemont, *Syst. Biol.* **2008,** *57,* 758-771.
[4] Z. H. Yang, *Mol. Biol. Evol.* **2007,** *24,* 1586-1591.
[5] D. Martinez, L. F. Larrondo, N. Putnam, M. D. Gelpke, K. Huang, J. Chapman, K. G. Helfenbein, P. Ramaiya, J. C. Detter, F. Larimer et al., *Nat. Biotechnol.* **2004,** *22,* 695-700.
[6] W. A. Doyle, A. T. Smith, *Biochem. J.* **1996,** *315,* 15-19.
[7] D. S. Moss, E. Naberdryk, J. Breton, W. Mäntele, *Eur. J. Biochem.* **1990,** *187,* 565-572.
[8] M. Sørlie, L. C. Seefeldt, V. D. Parker, *Anal. Biochem.* **2000,** *287,* 118-125.
[9] P. G. Furtmüller, J. Arnhold, W. Jantschko, H. Pichler, C. Obinger, *Biochem. Biophys. Res. Commun.* **2003,** *301,* 551-557.
[10] W. H. Koppenol, *Bioelectrochem. Bioenerg.* **1987,** *18,* 3-11.
[11] M. R. DeFelippis, C. P. Murthy, M. Faraggi, M. H. Klapper, *Biochemistry* **1989,** *28,* 4847-4853.
[12] G. Battistuzzi, M. Bellei, J. Vlasits, S. Banerjee, P. G. Furtmüller, M. Sola, C. Obinger, *Arch. Biochem. Biophys.* **2010,** *494,* 72-77.
[13] P. G. Furtmüller, J. Arnhold, W. Jantschko, M. Zederbauer, C. Jakopitsch, C. Obinger, *J. Inorg. Biochem.* **2005,** *99,* 1220-1229.
[14] J. Arnhold, P. G. Furtmüller, G. Regelsberger, C. Obinger, *Eur. J. Biochem.* **2001,** *268,* 5142-5148.
[15] H. Wariishi, L. Márquez, H. B. Dunford, M. H. Gold, *J. Biol. Chem.* **1990,** *265,* 11137-11142.
[16] T. Inubushi, E. D. Becker, *J. Magnet. Reson.* **1983,** *51,* 128-133.
[17] L. Banci, I. Bertini, R. Pierattelli, M. Tien, A. J. Vila, *J. Am. Chem. Soc.* **1995,** *117,* 8659-8667.
[18] L. Banci, I. Bertini, E. A. Pease, M. Tien, P. Turano, *Biochemistry* **1992,** *31,* 10009-10017.
[19] L. Banci, I. Bertini, P. Turano, M. Tien, T. K. Kirk, *Proc. Natl. Acad. Sci. USA* **1991,** *88,* 6956-6960.
[20] L. Banci, I. Bertini, P. Turano, J. C. Ferrer, A. G. Mauk, *Inorg. Chem.* **1991,** *30,* 4510-4516.
[21] L. Banci, S. Camarero, A. T. Martínez, M. J. Martínez, M. Pérez-Boada, R. Pierattelli, F. J. Ruiz-Dueñas, *J. Biol. Inorg. Chem.* **2003,** *8,* 751-760.
[22] I. Ayuso-Fernández, F. J. Ruiz-Dueñas, A. T. Martínez, *Proc. Natl. Acad. Sci. USA* **2018,** *115,* 6428-6433.
[23] F. J. Ruiz-Dueñas, M. Morales, E. García, Y. Miki, M. J. Martínez, A. T. Martínez, *J. Exp. Bot.* **2009,** *60,* 441-452.
[24] C. D. Millis, D. Cai, M. T. Stankovich, M. Tien, *Biochemistry* **1989,** *28,* 8484-8489.
[25] G. Battistuzzi, M. Bellei, F. De Rienzo, M. Sola, *J. Biol. Inorg. Chem.* **2006,** *11,* 586-592.
[26] C. Ciaccio, A. Rosati, G. De Sanctis, S. Marini, R. Santucci, P. Ascenzi, K. G. Welinder, M. Coletta, *J. Biol. Chem.* **2003,** *278,* 18730-18737.
[27] M. Oyadomari, H. Shinohara, T. Johjima, H. Wariishi, H. Tanaka, *J. Mol. Catal. B-Enzym.* **2003,** *21,* 291-297.
[28] R. E. Whitwam, R. S. Koduri, M. Natan, M. Tien, *Biochemistry* **1999,** *38,* 9608-9616.
[29] R. Santucci, C. Bongiovanni, S. Marini, R. del Conte, M. Tien, L. Banci, M. Coletta, *Biochem. J.* **2000,** *349,* 85-90.